RESEARCH ARTICLE

NANO · MICRO small
www.small-journal.com

Boron Nitride Nanosheets Induce Lipid Accumulation and Autophagy in Human Alveolar Lung Epithelial Cells Cultivated at Air-Liquid Interface

*Govind Gupta, Ziting Wang, Vera M. Kissling, Alexander Gogos, Peter Wick, and Tina Buerki-Thurnherr**

Hexagonal boron nitride (hBN) is an emerging 2D material attracting significant attention due to its superior electrical, chemical, and therapeutic properties. However, inhalation toxicity mechanisms of hBN in human lung cells are poorly understood. Here, cellular interaction and effects of hBN nanosheets is investigated in alveolar epithelial cells cultured on porous inserts and exposed under air—liquid interface conditions for 24 h. hBN is taken up by the cells as determined in a label-free manner via RAMAN-confocal microscopy, ICP-MS, TEM, and SEM-EDX. No significant ($p > 0.05$) effects are observed on cell membrane integrity (LDH release), epithelial barrier integrity (TEER), interleukin-8 cytokine production or reactive oxygen production at tested dose ranges (1, 5, and 10 µg cm^{-2}). However, it is observed that an enhanced accumulation of lipid granules in cells indicating the effect of hBN on lipid metabolism. In addition, it is observed that a significant ($p < 0.05$) and dose-dependent (5 and 10 µg cm^{-2}) induction of autophagy in cells after exposure to hBN, potentially associated with the downstream processing and breakdown of excess lipid granules to maintain lipid homeostasis. Indeed, lysosomal co-localization of lipid granules supporting this argument is observed. Overall, the results suggest that the continuous presence of excess intracellular lipids may provoke adverse outcomes in the lungs.

1. Introduction

Understanding biological interactions, cytocompatibility and cellular responses of nanomaterials is a prerequisite to address the safe use and regulatory acceptance of novel engineered nanomaterials, including the emerging two-dimensional (2D) materials.[1–4] 2D materials especially graphene or related materials are extensively exploited for numerous industrial and biomedical applications that include energy storage, superconductors, catalysts, drug delivery, and therapeutics.[5]

Hexagonal boron nitride (hBN) is a promising non-carbon 2D material that has received great attention in recent years for its potential applications in electronic and optoelectronic devices,[6,7] and as an outstanding thermal conductive material with higher chemical stability compared to metals.[8,9] In addition, hBN nanosheets or nanoparticles have been demonstrated as an excellent and promising alternative to elemental boron (B^{10}) in boron neutron capture therapy for cancer treatment.[10–13] hBN nanosheets provide higher accumulation efficiency as well as on-demand biodegradation in tumors than the elemental B^{10}, providing an opportunity for successful cancer therapy with the least off-target effects.[14–16] Besides cancer therapy, hBN coupled to serum protein has been used as a nanovector in adjuvant production to achieve immunomodulatory effects in mice.[17] Considering the extensive exploitation and use of hBN in many different application fields, including direct human exposure for medical treatment, it is of utmost importance to understand potential human health hazards early in the development of products.

Inhalation is one of the most relevant and sensitive exposure routes for engineered nanoparticles including 2D materials at workplaces.[18–20] Numerous studies evidenced the cytotoxic and immunomodulatory potential of some carbon-based 2D materials, including graphene oxides in lung cells in vitro and in vivo.[3,21–23] Boron nitride nanotubes (BNNTs), another boron nitride allotrope besides hBN, have also been shown to trigger cytotoxic effects in vitro and in vivo in mice lungs after inhalation exposure.[24–26] Pulmonary exposure to commercial or industrial-grade BNNTs in mice has been demonstrated to cause an acute inflammatory response in the lungs,[27,28] similar to the extensively studied toxic multi-walled carbon nanotube-7 (MWCNT-7 or MITSUI-7).[29,30] Furthermore, Kodali et al. (2017)[27] could show lysosomal destabilization, inflammasome

G. Gupta, Z. Wang, V. M. Kissling, A. Gogos, P. Wick, T. Buerki-Thurnherr
Laboratory for Particles-Biology Interactions
Swiss Federal Laboratories for Materials Science and Technology (Empa)
Empa, Lerchenfeldstrasse 5, St. Gallen 9014, Switzerland
E-mail: tina.buerki@empa.ch

The ORCID identification number(s) for the author(s) of this article can be found under https://doi.org/10.1002/smll.202308148

DOI: 10.1002/smll.202308148

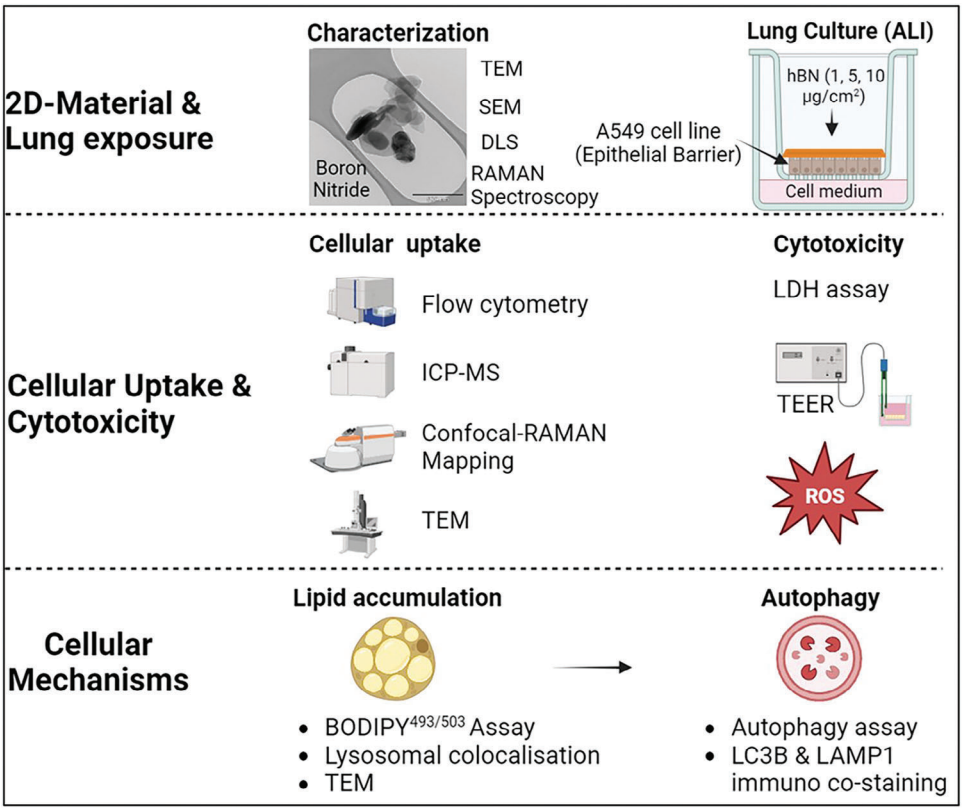

Figure 1. A schematic illustration of the study design. In vitro exposure and safety assessment of hBN in lungs using an air-liquid interface (ALI) models of alveolar epithelial cells (A549) cultivated to a confluent monolayer on a permeable support.

activation, and pyroptosis as potential cytotoxic mechanisms of BNNTs exposure in vitro (using THP1 cells) and in vivo. This cytotoxicity was not due to impurities introduced during the manufacturing of BNNTs (as is the case for carbon nanotube materials[31,32]) but is likely an inherent property of the BNNTs (e.g., high aspect ratio) since high-purity materials exhibited a greater cell membrane damage and higher cytotoxicity than those retaining manufacturing impurities (i.e., polymers).[33]

There have been limited and rather conflicting studies on biological interactions and cytotoxicity of hBN nanosheets. Similar to BNNTs, a recent study demonstrated that the shape of hBN nanosheets contributes to potential biological effects.[34] Authors could show that sharp-cornered (rhomboidal, cornered morphology) hBN nanosheets bind to the cell membrane of lung epithelial cells and create water channels across the lipid bilayer that facilitate their entry into lysosomes, followed by cathepsin B release and apoptotic cell death after lysosomal permeabilization. However, such adverse effects were not observed in the case of exposure to round-shaped hBN nanosheets. In another study, Lin et al. (2022)[35] demonstrated no significant effects of hBN exposure on cell viability or ROS production in primary human dendritic cells (DCs). However, they could show that hBN triggered the maturation of DCs followed by increasing the proliferation of T cells in the presence or absence of DCs.

Here, we performed a comprehensive assessment of the uptake, subcellular localization and cellular responses of hBN nanosheets in alveolar (A549) epithelial cells representing a simplified human alveolus cultivated on permeable supports under realistic air–liquid interface exposure conditions (**Figure 1**, schematics of the study design). A specific focus was set on potential toxicity mechanisms related to intracellular lipid accumulation and homeostasis in order to expand on previous work, which postulated an interference of hBN with membrane lipid bilayers in submerged lung epithelial cells.[34] All the experiments were conducted at occupationally relevant doses (1-10 µg cm^{-2}) based on potential lifetime exposure to nanomaterials in occupational settings.[36]

2. Results and Discussion

2.1. Characteristics of hBN Nanosheets

hBN nanosheets were obtained within the Graphene Flagship project consortium (https://graphene-flagship.eu/) and carefully characterized. The lateral primary size distribution of the particles was determined using transmission electron microscopy (TEM), revealing an average lateral diameter of 253.6 ± 110.9 nm for the single and multiple-layer hBN sheets (**Figure 2a**). The average hydrodynamic size of the particles measured with DLS in water and cell culture medium was 1670 ± 99 nm and 849 ± 46 nm, respectively (Figure 2b). The particles were observed to be less agglomerated and more stable in the cell culture medium possibly due to the presence of serum proteins.[37,38] The zeta potential

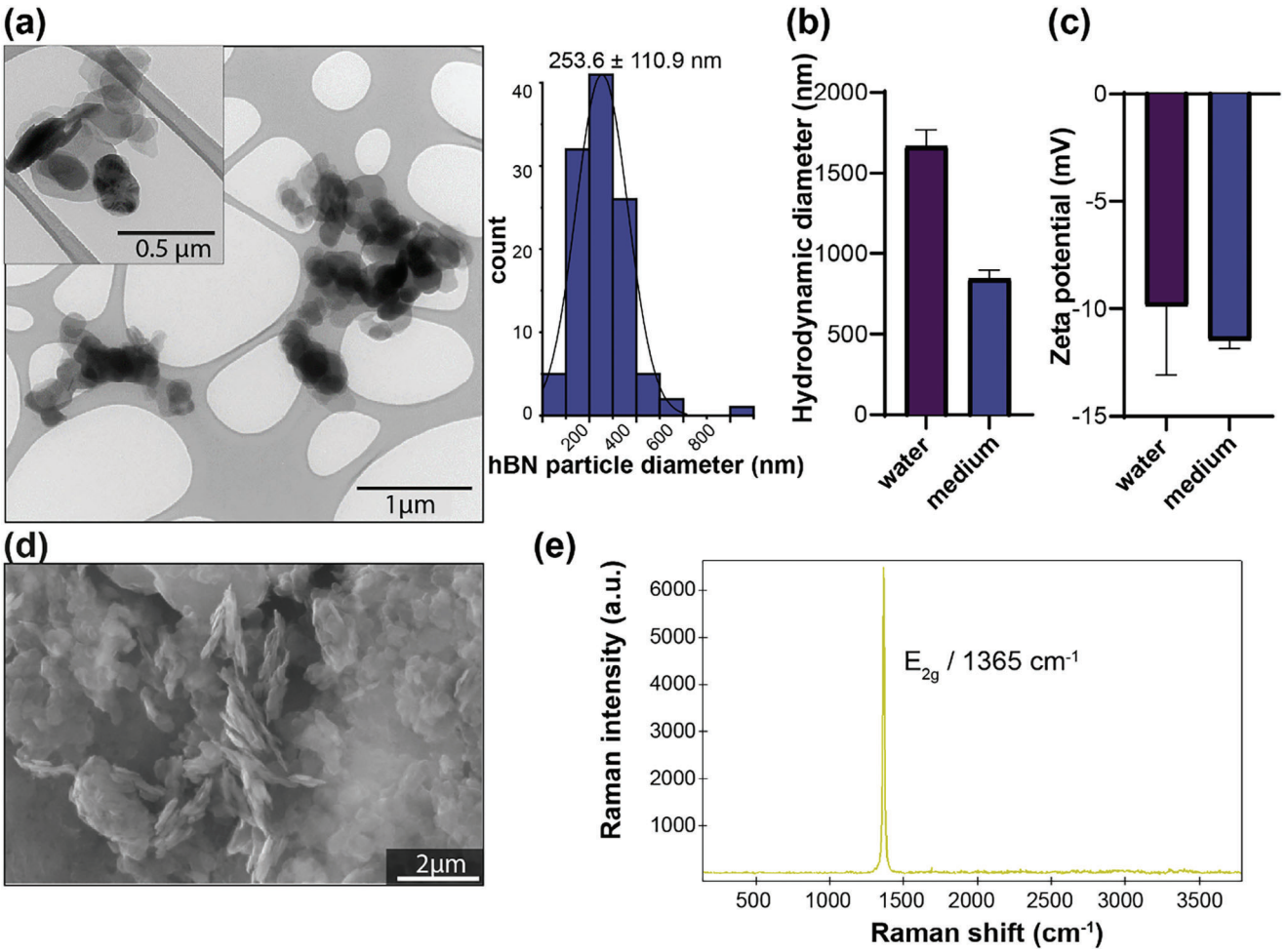

Figure 2. Characterization of hBN nanosheets. a) Representative TEM images of the particles in water and lateral primary particle diameter distribution determined from TEM micrographs for 112 distinguishable particles along their longest axis, revealing a mean lateral primary diameter of 253.6 ± 110.9 nm (± SD). Histogram with 100 nm binning and normal distribution fit. The inset image shows a higher magnification view of a few particles. b,c) Average hydrodynamic size (b), and zeta potential c), of the particles in water (Milli-Q) and cell culture medium (RPMI1640 with 10% FCS) determined by DLS. Data presented as mean ± SD from three independent measurements. d) SEM image indicates sheet-like morphology of hBN with round edges. e) Raman spectrum of thBN indicating the presence of a characteristic hBN peak at 1365 cm^{-1}. a.u.: arbitrary units.

of the particles was similar in water (−9.9 ± 3.1 mV) and cell culture medium (−11.5 ± 0.4 mV) (Figure 2c). Scanning electron microscopy (SEM), as well as the TEM micrographs of the particles showed particles with a dominantly round shape (Figure 2a,d). Raman analysis of the hBN powder disclosed the presence of a characteristic peak at 1365 cm^{-1} (Figure 2e). A similar peak was also shown by others for hBN nanosheets.[39,40] The particles were found endotoxin-free (0.095EU mL^{-1}) as determined by running a LAL assay.

2.2. hBN Nanosheets are taken up by Alveolar Epithelial Cells with Partial Co-Localization in Lysosomes

A549-ALI cultures were exposed to hBN for 24 h and uptake was determined by applying flow cytometry, ICP-MS, confocal-RAMAN scanning and transmission electron microscopy (TEM). The results are presented in **Figure 3**; Figure S1 (Supporting Information). Flow cytometry results showed a dose-dependent increase in the side scatter intensity (a proxy for cellular uptake) of hBN-exposed cells as compared to the untreated control (Figure S1, Supporting Information). Previous studies have also applied such a flow cytometry-based approach to measure the cellular uptake of carbon-based nanoparticles including 2D materials.[41–43] Furthermore, to quantify the intracellular boron content as a measure of hBN uptake/adhesion, we performed ICP-MS analysis of cells exposed to hBN (10 µg cm^{-2}) or boric acid (10 µg cm^{-2}-equivalent concentration of B) (Figure 3a). The B content was higher in the cells exposed to hBN as compared to boric acid controls suggesting different uptake mechanisms for ionic versus particle-bound B. Since the delivered cellular dose is key to determining the subsequent bioresponses, the toxicity of hBN will likely be different from its ionic counterparts. In this context, a higher uptake of certain metal/metal-oxide-based NPs (e.g., Cu and Ag NPs) than their ionic counterparts has been shown to modulate cytotoxicity.[44,45] However, the cytotoxicity of

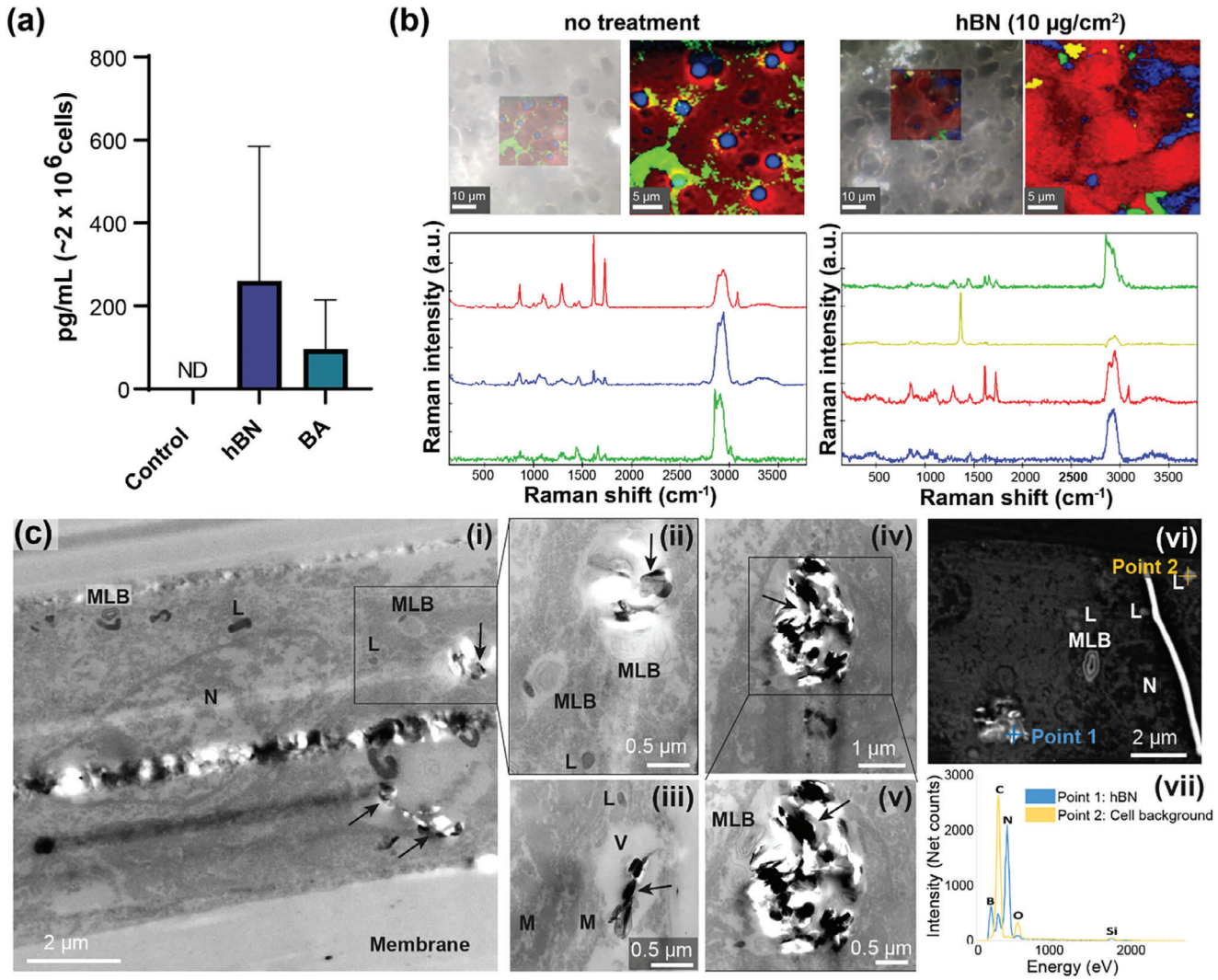

Figure 3. Cellular uptake of hBN in A549-ALI cultures after exposure for 24 h. a) Boron (B) content in cells after exposure to hBN (10 µg mL^{-1}) or equivalent concentration of boric acid (BA, ionic control). The boron content in the untreated cells (control) was below the detection limit (marked as not detected, ND). Data presented as mean ± SD (n = 3). b) Confocal-Raman scanning (scan area 30×30 cm^2) analysis indicates the presence of hBN in A549-ALI cultures. White arrows designate the presence of hBN in the exposed cells. Specific spectra at 1365 cm^{-1} correspond to hBN. a.u.: arbitrary units. c) i-v: TEM images of hBN-exposed cells cultivated on a transwell membrane show the accumulation of hBN (black arrows) in the cytosol next to cellular organelles such as multi-lamellar bodies (MLB), lysosomes (L) and mitochondria (M), and occasionally clearly inside cytotic vesicles (V) or phagosomes of intact cells (Figure 3d,iii), excluding the nucleus (N). The black-outlined images show higher magnification views of hBN accumulations at the specified region. Refer to Figure S3 (Supporting Information) for the corresponding TEM image of untreated (control) cells. vi-vii: SEM imaging and EDX point analysis of hBN accumulation inside cells cultivated on a transwell membrane indicate comparable intracellular localization of hBN accumulations as in TEM excluding the nucleus (vi), and confirm the high boron (B) and nitrogen (N) content of the hBN particles (blue point 1, vii), in contrast to electron-dense cellular structures (lysosome, orange point 2) with higher carbon (C) and oxygen (O) content. The Si content observed at both points stems from the Si-wafer support (vii).

the two NPs differed with respect to their salt counterpart. CuO NPs induced higher cell death and DNA damage compared to $CuCl_2$.[44,45] On the other hand, Ag had the opposite effect, where no toxicity (cell death) was observed for NPs, while $AgNO_3$ induced a high level of cell death.[45]

To understand whether intact hBN nanosheets are present in the cells after 24 h of exposure, we performed Raman spectroscopy on the cells (Figure 3b). For the reference of intact hBN, Raman spectra were recorded for pure hBN nanosheets deposited on a glass slide (Figure 2e). The hBN nanosheets showed a specific Raman peak at 1365 cm^{-1}, consistent with a previous study.[35] The same characteristic peak was determined from hBN particles in exposed cells following Raman mapping together with a cell-specific peak at ≈2800 cm^{-1} corresponding to biomolecules. The presence of hBN peak at 1365 cm^{-1} in the exposed cells confirms the occurrence of intact hBN after 24 h of exposure (Figure 3b). Furthermore, to visualize the intracellular localization of hBN nanosheets, we performed TEM and SEM-coupled energy-dispersive X-ray spectroscopy (EDX) analysis of cells (Figure 3c). TEM and SEM micrographs of hBN

(10 μg cm^{-2}) exposed A549 cells showed cellular uptake and an accumulation of hBN sheets in the cytosol next to cellular organelles such as multi-lamellar bodies and occasionally clearly inside cytotic vesicles or phagosomes of intact cells (Figure 3c,iii). A similar localization of hBN in the cytoplasm was also shown in a previous study using immune cells (dendritic cells).[35] We additionally analyzed these specific structures using SEM-EDX. Intracellular objects of this morphology showed elevated levels of both boron (B) and nitrogen (N), in contrast to other electron-dense structures found in the cells (Figure 3c,vi–vii). This additionally supports the interpretation that the observed structures were indeed intracellular hBN.

A recent study demonstrated lysosomal deposition of hBN (cornered morphology with lateral polar edges) in lung epithelial cells that eventually leads to cell death by causing lysosomal permeabilization followed by cathepsin B release.[34] On the other hand, round-shaped hBN nanosheets did not localize the lysosomes, therefore no toxicity was observed. To follow up on whether the hBN used in our study co-localizes and deposits in lysosomes, we labeled the hBN with green fluorescent (FITC) bovine serum albumin (BSA) protein by physical interaction of hBN nanosheets and FITC-BSA as illustrated in Figure S2a (Supporting Information). The A549-ALI cultures were then exposed to the FITC-BSA@hBN complex for 24 h and cellular uptake was confirmed again by measuring an increase in green fluorescence intensity with respect to untreated controls using flow cytometry (Figure S2b, Supporting Information). Next, the cells were co-stained with Lysotracker deep red and imaged under a confocal microscope. As shown in Figure S2c (Supporting Information), the particles (which appeared like nanosheets) with green fluorescence accumulated in the cells, with partial co-localization in lysosomes observed in a few cells as shown in the magnified image (Figure S2c, Supporting Information). In addition, confocal images showed heterogeneous uptake of labeled hBN in the cells, where hBN was not taken up by some cells. The partial co-localisation of label-free hBN (not with FITC-BSA) with lysosomes was also seen in TEM micrographs (Figure S2d, Supporting Information‘). Since the hBN used here has a round morphology, our data is in line with the previous study showing no lysosomal colocalization of such materials.[34] Overall, hBN nanosheets predominantly accumulated in the cytoplasm of lung alveolar epithelial cells with no potential sign of biotransformation (based on structural appearance in TEM and SEM, and confirmation of hBN peak in RAMAN spectra and SEM-EDX) observed up to 24 h.

2.3. hBN nanosheets do not Trigger Cytotoxicity, loss of Epithelial Barrier Integrity, Oxidative Stress or Interleukin-8 Release

To understand the cytocompatibility of hBN nanosheets in lung cells, A549-ALI cultures were exposed to 1–10 μg cm^{-2} of hBN for 24 h. hBN did not affect cell viability (based on LDH release) and only induced a slight but non-significant decrease of epithelial barrier integrity as determined by measuring the TEER value before and after hBN exposure (**Figure** 4a,b). In addition, hBN did not induce intracellular ROS production (Figure 4c) or lipid peroxidation at the tested dose range of up to 10 μg cm^{-2} (Figure 4d). Next, we evaluated whether hBN exposure in A549-ALI cultures induced cytokine/chemokine production. IL-8 is an oxidative stress-responsive proinflammatory cytokine constitutively produced by epithelial cells,[46,47] therefore, the release of IL-8 from hBN-exposed cells was measured. Results showed no significant ($p > 0.05$) increase in IL-8-release in hBN (10 μg cm^{-2}) exposed cells when compared with untreated control (Figure S4, Supporting Information). These results are in agreement with previous studies showing no cytotoxicity or oxidative stress after exposure to hBN nanosheets in human alveolar lung epithelial cells (A549 cells) or dendritic cells.[35,48] Recently, Lucherelli et al. 2021 have shown that the shape of hBN nanosheets plays a crucial role in their cytotoxicity in human lung epithelial cell line (H460 cells).[34] Only hBN with sharp edges but not with round edges triggered a dose-dependent (10–40 μg mL^{-1}) cytotoxic effect. By applying molecular dynamics (MD) simulations, they could further show that such effects of sharp-edged hBN were observed due to the formation of cross-membrane water channels in the lipid bilayer membrane that facilitated their cellular entry and lysosomal permeabilization. Similar to sharp-edged hBN nanosheets, the toxicity of BNNTs has also been proposed to be driven by piercing the cell membrane[26] and/or by extraction of lipids from lipid bilayer membranes.[49] Taken together, boron nanoparticle toxicity appears to be governed by the presence of sharp edges. SEM and TEM images of hBN nanosheets used in our study showed the absence of sharp edges, which could explain the overall low cytotoxicity on A549-ALI cultures (Figure 2a,d).

2.4. hBN Nanosheet Exposure Leads to Lipid Accumulation in Human Alveolar Epithelial Cells

Dysregulation of lipid homeostasis in the lungs could be a cause of pulmonary diseases in children or adults.[50,51] The alveolar type II cells are one of the most active cell types in the lungs with a high lipid metabolism.[51] These cells regularly produce and degrade surfactant lipids (i.e., dipalmitoylphosphatidylcholine) that are essential for lowering respiration-mediated surface tension in the alveoli and maintaining the respiratory system.[52,53] Therefore, any effects on lipid homeostasis in alveolar lung cells may contribute to the development of pulmonary illness. Here, we examined whether exposure to hBN nanosheets in A549-ALI cultures (type II alveolar cells) could affect lipid accumulation. To this end, we probed the cells with Bodipy493/503, a lipophilic green fluorescent dye that stains neutral lipids in the cells including in lipid granules (e.g., lipid droplets).[54] Lipid granules are the dynamic cytosolic organelles involved in buffering excess lipids in the cells to maintain lipid homeostasis.[55–57] Interestingly, semi-quantitative analysis of lipid accumulation (based on a change in Bodipy493/503 fluorescence) in cells using flow cytometry demonstrated a relatively dose-dependent (1 – 10 μg cm^{-2}) increase in lipid accumulations after 24 h of exposure to hBN when compared with the untreated control (**Figure** 5a). To localize the lipid accumulation, we performed confocal imaging of the cells followed by transmission electron microscopy. As shown in Figure 5b, the lipid accumulation in the cells mainly occurred in the lipid granules, which increased in their number after exposure to hBN (10 μg cm^{-2}) for 24 h. TEM images further confirmed the increased presence of lipid granules

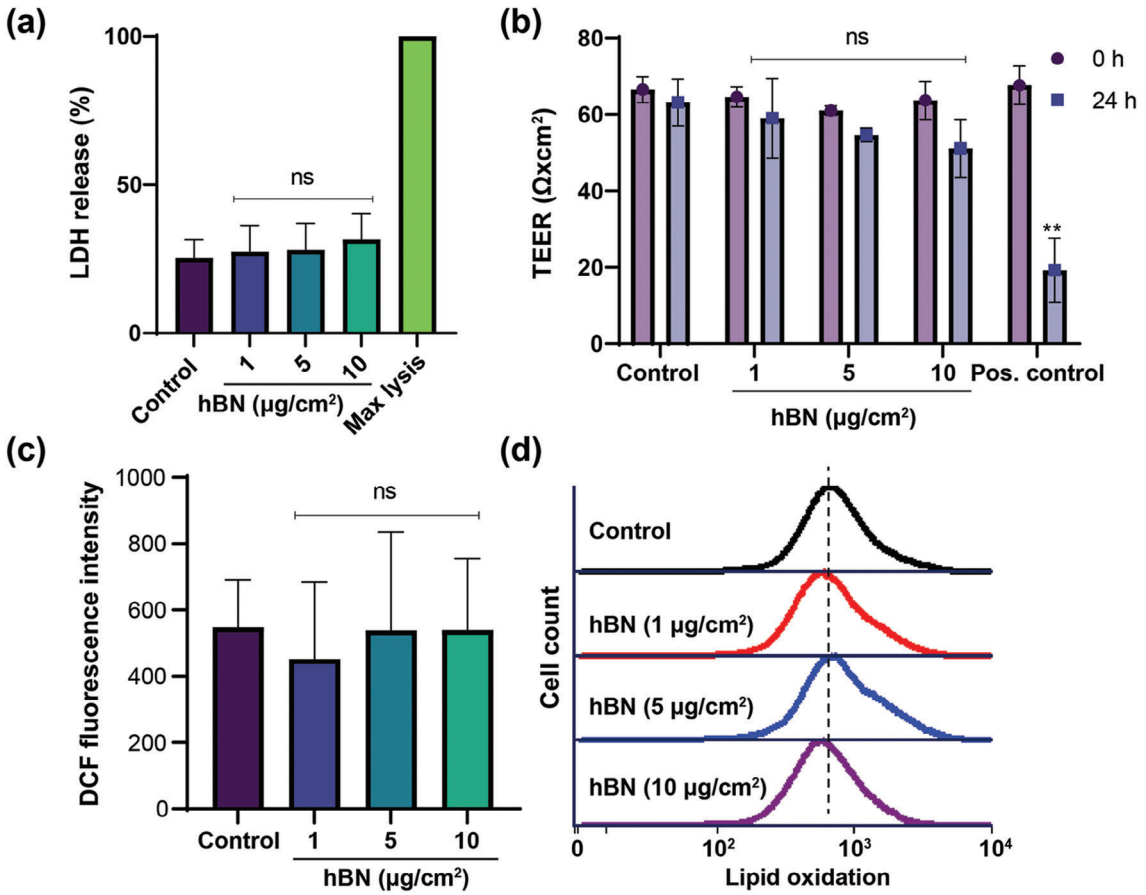

Figure 4. Cytotoxicity and oxidative stress in A549 cells after 24 h of hBN exposure. a,b) No cytotoxicity or loss of barrier integrity was observed in cells as determined by measuring LDH release (a), and TEER (b), respectively. c) No change in cellular total ROS content was observed as determined by the DCF assay. Data presented as mean ± SD (n = 3). $^{**}p < 0.01$ is statistically significant with respect to control. $p > 0.05$ considered statistically not significant (ns). *p*-value was calculated by applying One-way ANOVA and Dunnett's multiple comparison test for post hoc analysis. d) No effect in cellular lipid oxidation was observed as measured by C11-BODIPY(581/591) staining of the cells. The dotted line indicates no notable shift in green fluorescence intensity (reflecting to lipid oxidation) to the right between control and the different treatments. The lipid oxidation experiment was repeated twice with similar observations and a representative histogram is presented.

in hBN-exposed cells (Figure 5c). Although this is, to our knowledge, the first demonstration of intracellular lipid accumulation in lung epithelial cells from hBN exposure, previous studies have shown similar effects for other nanoparticles. For instance, metal or metal oxide nanoparticles have been shown to modulate cellular lipid homeostasis and metabolism in rats and mice.[58,59] Furthermore, Ma et al. (2021)[60] could demonstrate the effect of amorphous silica nanoparticles (known biocompatible material with no pronounced cytotoxicity) on lipid metabolism in RAW 264.7 macrophage cell lines by proteomic analysis of lysosomes. They also observed an accumulation of cholesterol lipids in the cytosol which co-localized with lysosomes. Since lysosomes perform a crucial role in the breakdown of excess or abnormal cellular lipids,[61] it is important to investigate their potential contribution towards nanoparticle-induced toxicity, especially those involving disturbances in lipid metabolism.

Therefore, to further understand whether lysosomes are potentially involved in the breakdown of hBN-induced lipid changes in A549-ALI culture, we co-stained the lipid granules and lysosomes using BODIPY$^{493/503}$ and Lysotracker deep red, respectively. The confocal micrographs showed a co-localization of lipid granules and lysosomes only in some cells of hBN-exposed (10 μg cm^{-2}) cultures, however, co-localization was not seen in control cells (Figure 5d). Despite the low co-localization of lipid droplets and lysosomes, we performed further studies on autophagy to better understand the potential role of lysosomes towards the observed toxicity of hBN on lipid homeostasis.

2.5. hBN Nanosheet Exposure Induces Autophagy in Human Alveolar Epithelial Cells

Autophagy is a lysosome-dependent cellular degradation mechanism that could play a protective function under stress in the lung.[63–65] Singh et al. (2009)[66] uncovered the crucial function of autophagy in regulating the intracellular stores of lipids (termed lipophagy) and eventually maintaining lipid homeostasis. Others have also identified autophagy as a potential caretaker of cellular lipid homeostasis and its associated cellular functions.[67,68] A recent study demonstrated an impaired

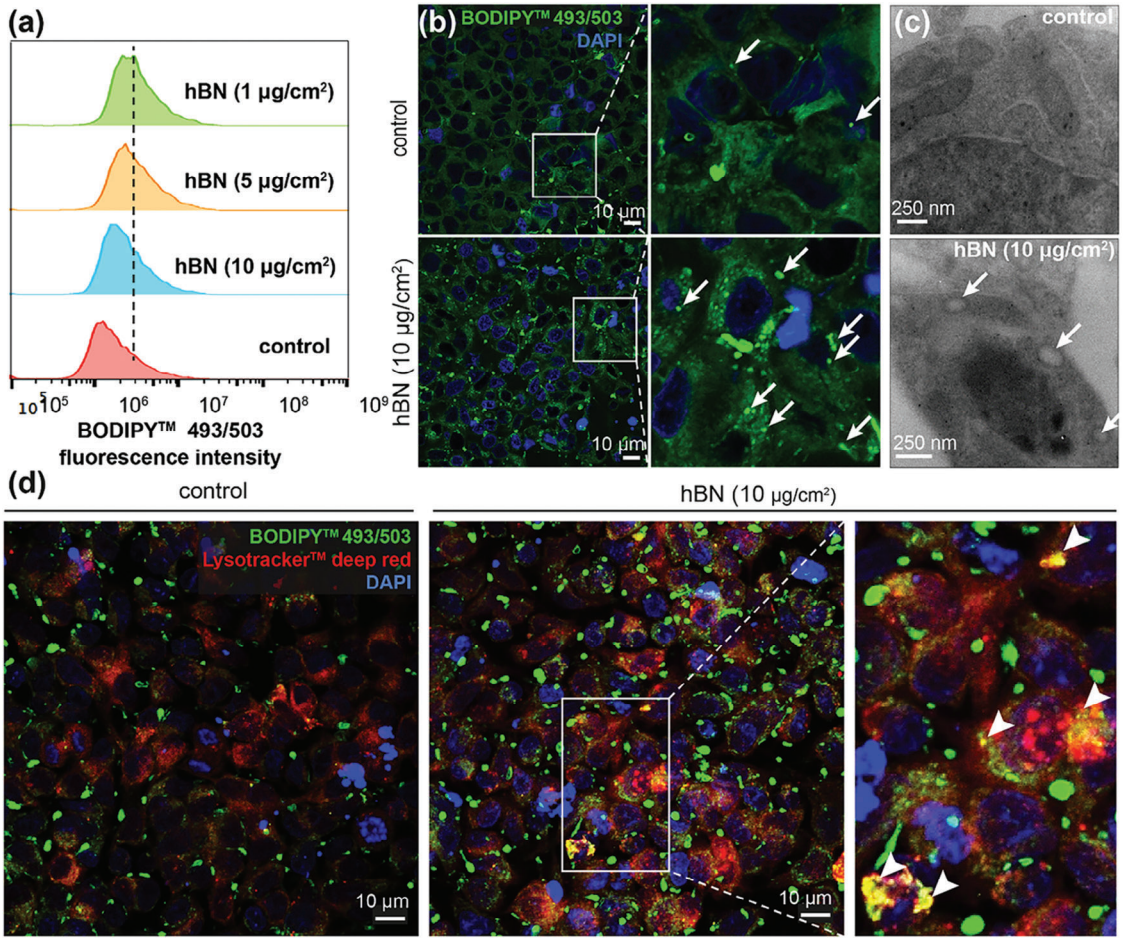

Figure 5. Lipid accumulation in A549 cells after hBN exposure for 24 h under ALI conditions. a) A dose-dependent increase in BODIPY$^{493/503}$ fluorescence intensity in the cells was determined using flow cytometry. b) Confocal micrographs confirmed the accumulation of lipids in the lipid granules (white arrows in the magnified images). The flow cytometry and confocal imaging experiments were repeated three times (n = 3) and a representative histogram or image was presented. c) Representative TEM micrographs show the presence of lipid granules with their characteristic thin dark outline (see, e.g.,[62]) in the cytosol (white arrows). Note that the control and hBN-treated cells were inevitably cut at different cellular z-axis depths, making the control cells appear larger at the same magnification. d) Lysosomal co-localization of lipid granules in hBN-exposed cells at the indicated concentration. Arrowheads in the magnified image indicate the yellow/orange puncta in cells formed due to the co-localization of lipid granules (green, BODIPY$^{493/503}$) with lysosomes (Lysotracker deep red).

lysosomal function and autophagy in human alveolar epithelial cells upon exposure to silica nanoparticles, leading to fibrosis and cell death.[69] However, reverting the lysosomal function and autophagy protected the cells from fibrosis and cell death confirming the protective function of autophagy in lung cells. Therefore, we investigated whether the accumulation of lipid granules could induce autophagy in hBN-exposed A549-ALI cultures. Our results showed a dose-dependent (5-10 µg cm^{-2}) and statistically significant ($p < 0.05$) increase in autophagy after 24 h of exposure to hBN (**Figure** 6a,b). Moreover, confocal micrographs revealed a higher number of autophagic vacuoles in cells exposed to 10 µg cm^{-2} hBN compared to untreated controls (Figure 6c). Rapamycin, a known autophagy inducer, also triggered autophagy response in the cells.

We further validated autophagy induction in cells by measuring the accumulation of LC3B-positive punctuated structures and then explored the autophagy flux by co-staining the cells with lysosomal-associated membrane protein 1 (LAMP-1) (**Figure** 7a). The immunofluorescence images of cells revealed an increased presence of LC3B -positive punctuated structures in hBN-exposed cells, confirming the accumulation of autophagosomes after 24 h (Figure 7a). Following autophagosome formation, the next step in autophagy process involves their fusion with lysosomes (known as autophagolysosomes) and then subsequent degradation of the cargo. However, an impairment in the function of lysosomes could lead to the accumulation of autophagosomes in the cells. Therefore, we evaluated autophagosome-lysosome fusion by observing the co-localization of LC3B (green puncta) and LAMP1 (red puncta) in the cells. The results showed an enhanced autophagosome formation (LC3B positive green puncta) with some colocalization of LC3B with LAMP1 (yellow puncta, autophagolysosomes) in hBN-treated cells, suggesting that lysosomal degradation of autophagosomes was partially decreased but not completely impaired (Figure 7a), Chloroquine was used as a positive control for autophagy flux since it is known to block the fusion

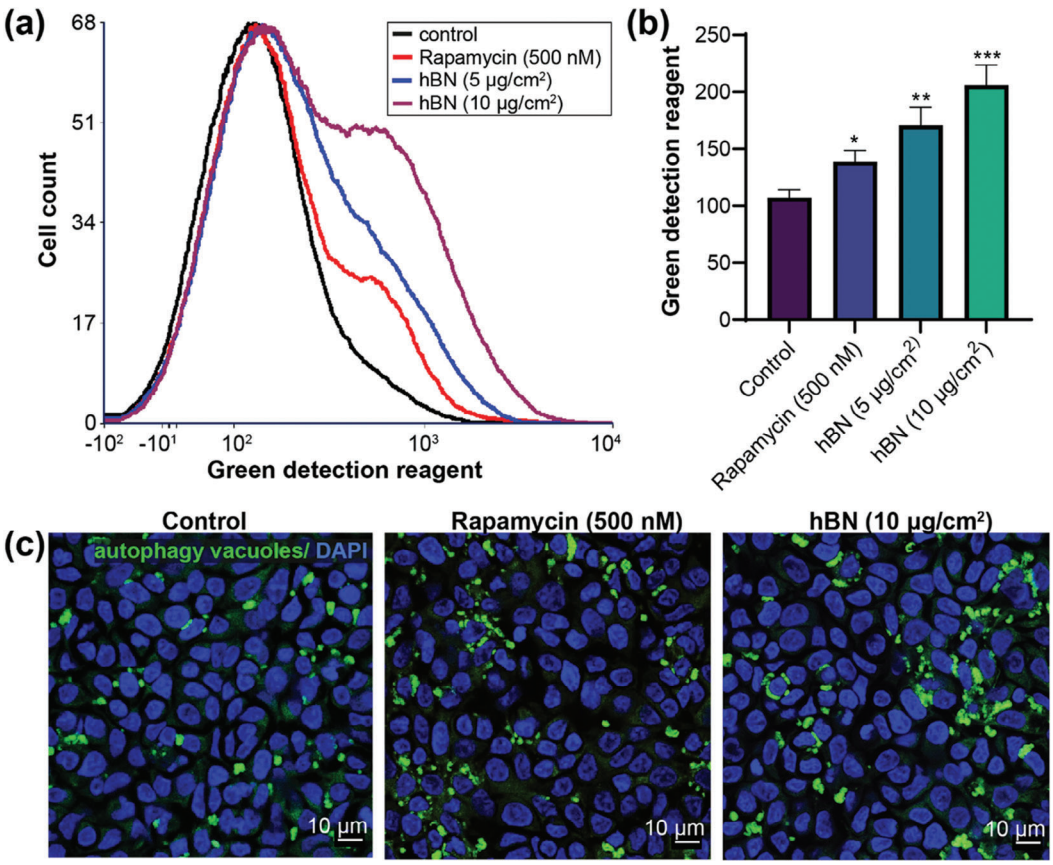

Figure 6. Autophagy induction in A549-ALI cultures after exposure to hBN nanosheets for 24 h. a,b) Flow cytometry measurements showed a dose-dependent increase in the cellular fluorescence intensity of the green-detection reagent corresponding to autophagy induction in cells, a) representative histogram overlay, and b) median cellular intensity of green-detection reagent presented as mean ± SD (n = 3). Rapamycin is used as a positive control to induce autophagy in cells. $*p < 0.05$, $**p < 0.01$, $***p < 0.001$ are statistically significant with respect to untreated control. *p*-value was calculated by applying One-way ANOVA and Dunnett's multiple comparison test for post hoc analysis. c) Confocal micrographs indicate an increase in the accumulation of autophagy vacuoles (green) in the cells after exposure to rapamycin or hBN nanosheets at indicated concentrations. Scale bar: 10 µm.

of lysosomes with autophagosomes.[70] As expected, autophagosome accumulation was increased in chloroquine-exposed cells (Figure 7a). Next, we examined whether inhibiting autophagy using a pharmacological inhibitor (wortmannin) could affect hBN cytotoxicity in lung cells. Wortmannin is a phosphatidylinositol 3-kinase inhibitor widely used for inhibiting cellular autophagy.[71] The results showed a slight increase ($p > 0.05$) in cytotoxicity of hBN (10 µg cm^{-2}) nanosheets in the cells pre-incubated with wortmannin with respect to control (or only wortmannin exposed cells), indicating a protective function of autophagy in hBN-exposed cells (Figure 7b). In a recent study, Wei et al. (2021)[72] demonstrated that dietary exposure to copper ions in catfish increased lipid deposition, which was reverted to normal levels by induction of lipophagy upon subsequent exposure to zinc. Others have also demonstrated the protective role of lipophagy or autophagy to counteract abnormal lipid accumulation and lipotoxicity in cells.[73–75] Taken together with the results obtained in the study, our current model (depicted in Figure 7c) potentially suggests that hBN exposure enhances the accumulation of lipid granules in alveolar lung cells, followed by activation of autophagy. Next. the excess lipid granules undergo autophagy-mediated degradation (also known as lipophagy) that subsequently protects cells from lipotoxicity and enhances cell survival. On the other hand, continuous production of lipid granules due to the biopersistence of hBN in the cells may ultimately decrease the lysosomal function or lead to lysosomal insufficiency, which could be a potential cause for the accumulation of autophagosomes observed in our study.

Therefore, a long-term exposure study is needed for a complete hazard assessment of hBN, and our study emphasizes the importance of placing a specific focus on the impact of chronic hBN exposure on lipid metabolism and homeostasis.

3. Conclusion

Hexagonal boron nitride is a promising 2D material exploited for a wide range of applications in biomedical, therapeutic, energy and electronic sectors. However, the potential impact of hBN exposure on lung cells and its toxicity mechanisms have not been well studied. In the present study, we have demonstrated cellular uptake and subtoxic effects of hBN nanosheets in lung alveolar epithelial cells and further explored the mechanism of subtoxic

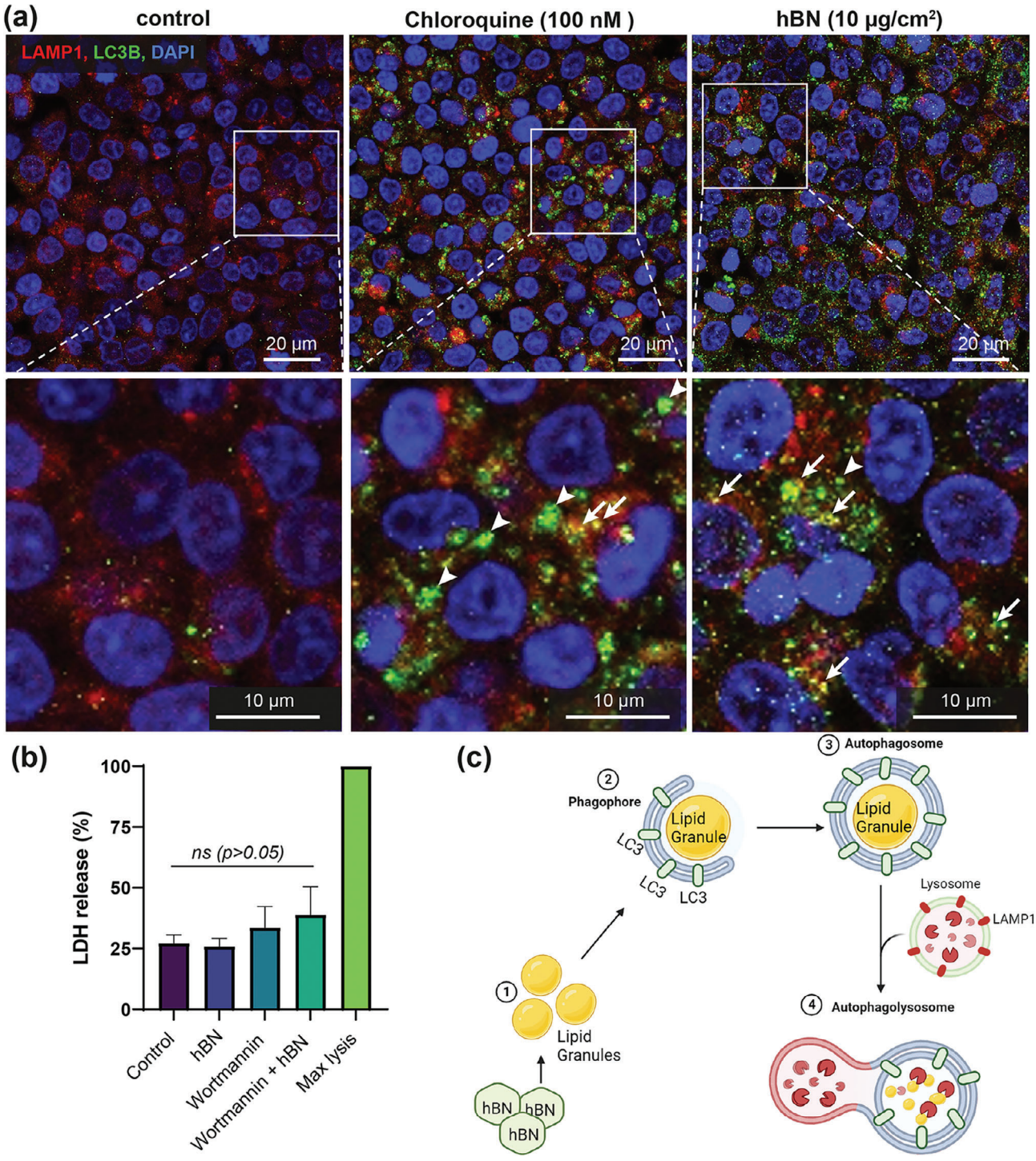

Figure 7. Autophagy flux in hBN (10 µg/cm^2) exposed A549-ALI cultures after 24 h. a) Immunofluorescence images of lung cultures with a zoomed section showing a few cells from corresponding regions (white square) of the image to indicate enhanced accumulation of LC3B-positive (green punta) autophagosomes (arrowheads) in chloroquine (positive control) or hBN-exposed cells. Few autophagosomes were seen to be co-localized with lysosomes (LAMP1-positive, LC3B-positive, yellow punctae) forming autophagolysosomes (white arrows). Immunofluorescence experiments were repeated at least twice in replicates and representative images are shown here. b) Pre-incubation of cells with autophagy inhibitor wortmannin (100 nM) slightly (not statistically significant, $p > 0.05$) improved the cytotoxicity of hBN as indicated by an increase in LDH release. Data presented as mean ± SD (n = 3). $p > 0.05$ considered statistically not significant (ns). *p*-value was calculated by applying One-way ANOVA and Tukey's multiple comparison test for post hoc analysis. (c) Schematic Figure depicts the current model of hBN-triggered cellular autophagy. hBN is taken up by alveolar lung cells leading to the induction of lipid granules. Excess production of cellular lipid granules activates autophagy, which degrades the lipid granules to maintain cellular lipid homeostasis. However, continuous production of lipid granules may reduce lysosomal function, resulting in autophagosome accumulation in the cells.

responses in the cells. Our results show that hBN nanosheets did not affect cell viability and epithelial barrier integrity of A549-ALI cultures after 24 h exposure to a dose range of 1–10 μg cm^{-2} despite being taken up by the cells. However, the observed subtoxic effects of hBN on lipid homeostasis and subsequent induction of autophagy could be of potential concern. In particular, long-term and/or repeated exposure to hBN may "overload" the autophagy-mediated protective function of the lung cells and may give rise to delayed adverse effects or even lead to the development of lipid-mediated lung diseases (i.e., asthma and COPD). This study recommends future investigations on the long-term impact of hBN exposure and its correlation to chronic lung diseases.

4. Experimental Section

Material Dispersion and Characterization: The exfoliated hBN nanosheets were obtained in powder form from the Graphene Flagship consortium (Provider: BeDimensional, Italy). For the cell experiments, a dispersion of hBN nanosheets was prepared in endotoxin-free BSA water (0.1%). Briefly, 2 mg of hBN powder was weighed in a sterile vial followed by adding 4 mL of BSA water (0.1%) to achieve a 0.5 mg mL^{-1} stock suspension. The particles were vortexed briefly and sonicated using a bath sonicator for 15 min followed by another 15 min, before use. Stock dispersions were diluted in a cell culture medium for exposure or in water for characterization to the final working experimental concentrations (1–10 μg cm^{-2}). The characterizations were performed using the following techniques:

Material Dispersion and Characterization–Transmission Electron Microscopy (TEM): Morphology and primary particle size of hBN were investigated using TEM. Briefly, 5 μL of 50 μg mL^{-1} hBN nanosheets in water were drop-casted onto a 200-mesh copper grid with holey carbon film (Electron Microscopy Resolutions, HC200Cu). Then the grid was air-dried before imaging with a Zeiss EM 900 microscope at 80 kV (Carl Zeiss Microscopy GmbH, Germany). The primary particle diameters were measured for 112 hBN particles (that were distinguishable inside agglomerates) along their longest axis with the TEM user interface iTEM 5.1 software (Build 1700, Olympus), plotted and statistically analyzed using Origin 2022.

Material Dispersion and Characterization–Scanning Electron Microscopy (SEM): For SEM analysis, hBN nanosheets dispersed in BSA water were filtered onto anodized Al-oxide disk filters (TedPella, USA) and dried. SEM imaging was performed using an Axia ChemiSEM (Thermo Fisher Scientific).

Material Dispersion and Characterization–Zeta Sizer: Hydrodynamic size and z-potential of hBN (50 μg mL^{-1}) in water and complete cell culture medium (containing 10% FBS) were determined using a Zetasizer Nano ZS instrument (Malvern Instruments, UK).

Material Dispersion and Characterization–RAMAN Spectroscopy: Raman spectrum of the exfoliated hBN particles was obtained using a WITec Alpha 300 RAS system (Oxford Instruments, Germany) equipped with a 532 nm and 488 nm excitation laser. For the measurement, a thick layer of hBN nanosheets was prepared in a glass slide and then a single-point spectrum was recorded using a 532 nm laser.

Material Dispersion and Characterization–Endotoxin Chromogenic Assay: The endotoxin concentration in hBN suspension (100 μg mL^{-1}) was measured using the Pierce LAL Chromogenic Endotoxin Quantitation kit (sensitivity 0.1 EU mL^{-1}; Thermo Fisher Scientific, USA), following the manufacturer's instructions.

Air-Liquid Interface Culture of Alveolar Epithelial Cells (A549-ALI Culture) and hBN Exposure: Human alveolar pulmonary epithelial cells (A549) were obtained from the American Type Culture Collection CCL-185, Lot number 60 120 896) and were cultured and maintained in RPMI-1640 (Rosewell Park Memorial Institute-1640 medium, Sigma-Aldrich) medium supplemented with 10% fetal calf serum (Gibco, Germany), 1% L-glutamine (Gibco, Germany), and 1% penicillin-streptomycin (Gibco, Germany). The cells were sub-cultured regularly and maintained at 37 °C in the CO_2 (5%) incubator. For the experiments, the A549 cells (2.5×10^5) were seeded on the apical side of microporous transwell inserts (PET, pore diameter 3 μm, 113.1 mm^2 growing area, Thincerts, Greiner Bio-One Vacuette Schweiz GmbH, Switzerland), and cultured for five days at submerged condition (0.5 mL and 1.5 mL of cell medium at apical and basolateral sides, respectively). To establish the air-liquid interface (ALI) environment, the cell culture medium was removed from both apical and basolateral sides after five days and replenished with fresh medium only at the basolateral side. The cells were maintained at ALI conditions for another 24 h. Cells were then exposed to the hBN (1, 5, or 10 μg cm^{-2} corresponding to 10.3, 56.65, or 113.3 μg mL^{-1}) or other tested materials by dropping 100 μL of suspensions at the apical side of the cultures for 24 h unless otherwise noted. Triton-X-100 (0.2%; Sigma-Aldrich) was used as a positive control for cytotoxicity assay and added to the cultures only for 2 h.

Cellular Uptake and Subcellular Distribution of hBN–Flow Cytometry: Flow cytometry was applied to evidence the cellular uptake of hBN in A549 cells based on measurement of side scatter (SSC) intensity in the hBN-exposed cells with respect to control after 24 h. After exposure, the cells were dissociated from transwell membranes by incubating in 1x Trypsin (0.025%) (Gibco, Germany) for 15 min. The single-cell suspension of dissociated cells was analyzed using an Attune flow cytometer operating with Attune software (ThermoFisherScientific, U.S.A.). Data were analyzed using FCS Express software.

Cellular Uptake and Subcellular Distribution of hBN–RAMAN-Confocal Mapping: Raman spectroscopy and confocal mapping were carried out using a WITec Alpha 300 RAS system (Oxford Instruments, Germany) equipped with a 532 nm and 488 nm excitation laser. The measurements were performed using a 50x ZEISS LD EC Epiplan-Neofuar Dic 50x/NA 0.55 objective and with a 532 nm laser. Laser power was optimized and set to 10 mW to minimize heat-induced effects in the cells. The spectrometer diffraction grating of 600 L mm^{-1} was implemented. First, the cultures were exposed to the hBN (10 μg cm^{-2}) as indicated for 24 h. Following exposure, the cultures were washed with phosphate buffer saline (1x PBS, Gibco) and fixed using Histofix (4% formaldehyde, Sigma-Aldrich, Germany) for 15 min and washed again with PBS. Next, the cultures with transwell membranes were mounted in the glass slides using Mowiol 4–88 (Sigma-Aldrich) and left overnight at 37 °C for curing. The Raman spectrum of hBN alone was also recorded as a reference. For the Raman mapping, a Raman spectrum was recorded in every image pixel. Raman maps indicating hBN intensity distributions were reconstructed using true component analysis. All spectra were analyzed using WITec Project Plus 6.1 software (Oxford Instruments, Germany) using cosmic ray removal and baseline correction filters.

Cellular Uptake and Subcellular Distribution of hBN–Inductively Coupled Plasma Mass Spectrometry (ICP-MS): For quantitative analysis of cellular uptake, A549-ALI cultures were exposed to 10 μg/cm^2 of hBN or boric acid (equivalent concentration) for 24 h as described above. Following exposure, the transwell membrane from ALI cultures was collected and processed for boron analysis using ICP-MS. The samples were predigested in 1 mL of concentrated HNO_3 (65-67%, puriss. p.a. grade, Sigma Aldrich, Germany) and 0.2 mL of H_2O_2 (30%. EMSURE, Supelco, Switzerland) for at least 72 h at room temperature (RT) followed by a pressurized microwave (turboWAVE 1500 MWS GmbH, Germany) digestion at 1000 W, 200°C, and 150 bar pressure for 40 min to ensure complete mineralization. Before analysis, all the samples were diluted to reach ≈2% of HNO_3. For all samples, boron (^{11}B isotope) was quantified using an Agilent 7900 ICP MS (Agilent, USA) instrument. Calibration standards of 0.01, 0.5. 0.1, 1, 5, and 10 μg L^{-1} B were prepared in 2% HNO_3 using a certified 1000 mg/L B reference standard (MSB-100PPM, Inorganic ventures, Suisse Technology Partners, Switzerland). The isotope ^9Be at a concentration of 100 μg L^{-1} was used as an internal standard to correct for non-spectral interferences and was always mixed online with the standards and samples at a ratio of 1:10 using a T-piece. For quality assurance, a reference material with a certified B concentration of 158 μg L^{-1} was measured along with the samples (IV Stock 1643 Trace elements in water, Inorganic ventures) and the recovery for B was 98%. The results were presented as pg/mL B in

approximately two million cells. The average number of cells in transwell inserts was pre-determined by counting at least three independent transwells following trypsinizing. The average number of cells in each transwell insert was ≈2 × 10^6, which was further used in the calculation of total cellular B content.

Cellular Uptake and Subcellular Distribution of hBN–Transmission Electron Microscopy: To visualize hBN intracellularly, A549-ALI cultures were exposed to hBN (10 µg cm^{-2}) for 24 h. After exposure, the samples were collected and processed for TEM analysis. First, the transwell cultures were washed three times with sterile 1x PBS (Gibco) and fixed with 3% glutaraldehyde (Sigma-Aldrich, Germany) prepared in 0.1 M Na-Cacodylate buffer (Electron Microscopy Sciences, U.S.A.) for 25 min at RT, and with fresh fixative for 40 min at 4 °C and then 20 min again at RT. The transwell cultures were washed twice for 20 min with 0.2 M Na-Cacodylate buffer (Electron Microscopy Sciences, pH 7.4), once at RT and once at 4 °C. Following postfixation and contrasting with 2% OsO_4 (Electron Microscopy Sciences) in 0.1 M Na-Cacodylate buffer for 1.5 h at RT, the cultures were washed with ultrapure water at 4 °C and then serially dehydrated at 4°C with an ethanol gradient (50%, 75%, 100% from HoneyWell, Riedel-de-Haen, 100% water-free from Sigma-Aldrich). The transwell membranes were cut out from the culture inserts using a scalpel and immersed into 100% water-free acetone (Sigma-Aldrich, Germany) at RT, followed by an Epon gradient in water-free acetone (33% at 4 °C overnight, 66% at 4 °C for 6 h, 100% at RT for 2 h) using Epon 812 substitute resin (Epoxy embedding kit 45 359, Sigma-Aldrich, Germany). The transwell membranes were cut into smaller pieces using scissors, embedded in molds with fresh 100% Epon and cured in the oven at 60 °C for at least 2 days. Ultrathin sections (80-100 nm) were cut using an ultramicrotome (Leica EM UC6, Germany) and placed onto Formvar-coated copper grids (200-mesh, EM Resolutions). The samples were examined with a Zeiss EM 900 microscope (Carl Zeiss Microscopy GmbH, Germany) at 80 kV.

Cellular Uptake and Subcellular Distribution of hBN–Scanning electron Microscopy and Elemental Analysis: For SEM imaging of intracellular hBN and elemental analysis with energy-dispersive X-ray spectroscopy (EDX), 200 nm-thick sections of the transwell membranes embedded as Epon blocks were cut using an ultramicrotome as described above for TEM and placed onto a silicon wafer (Tedpella, U.S.A.). The Si-wafer was pretreated with 30% NaOH for 5 min and subsequently washed using ultrapure water to promote hydrophilicity of the wafer surface. SEM imaging and EDX analysis were performed using an Axia ChemiSEM (Thermo Fisher Scientific, U.S.A.) in beam deceleration mode with a concentric backscatter detector (CBS) at 3 kV landing energy.

Cellular Uptake and Subcellular Distribution of hBN–FITC-BSA Labeling of hBN and Lysosomal Colocalization: For FITC-BSA coating, hBN (0.5 mg mL^{-1}) and 0.1% FITC-BSA (Sigma-Aldrich, Germany) were mixed in water and bath sonicated for 30 min, followed by vigorous vortexing for 1 min before and after sonication. hBN and FITC-BSA suspension was then left overnight at RT. Next, the suspension was centrifuged at 25 000 xg for 1 h at 4 °C to remove free (unbound) FITC-BSA. The supernatant was discarded and the pellet, containing hBN coated with FITC-BSA (referred to as FITC-BSA@hBN hereafter) was re-dispersed with an equal amount of sterile endotoxin-free water and used further in the experiments. A similar labeling approach using FITC-BSA has been used by others for amorphous silica nanoparticles.[60] For uptake measurement of FITC-BSA@hBN in A549 cells, flow cytometry measurement of cells was performed exposed at 10 µg cm^{-2} FITC-BSA@hBN for 24 h. After exposure, the samples were collected as described above and the green fluorescence (corresponds to FITC) intensity was recorded using an Attune flow cytometer operated with Attune software (ThermoFisherScientific, U.S.A.). Data were analyzed using FCS Express software.

For analysis of lysosomal co-localization of FITC-BSA@hBN, the cells were co-stained with LysoTracker deep red (ThermoFisherScientific) and images were captured using a confocal laser scanning microscope (CLSM; LSM 780, Zeiss, Germany). Briefly, the A549-ALI cultures were washed thrice with PBS and incubated with 100 nM of LysoTracker deep red for 30 min followed by 4′,6-diamidino-2-phenylindole (DAPI) for another 15 min. After staining, the cells were washed again and fixed with Histofix (4% formaldehyde, Sigma-Aldrich, Germany) for 15 min. After fixation, the samples were mounted on glass slides using Mowiol 4–88 (Sigma-Aldrich, Germany) and left overnight at 37°C.

Cytotoxicity and Oxidative Stress Assays–Lactate Dehydrogenase (LDH) Release Assay: LDH release from the cells indicates the loss of cellular (plasma membrane) integrity and was used to measure the cytotoxicity of hBN in A549-ALI cultures after 24 h. Triton-X-100 (0.2%) was applied for 1 h as the positive control for LDH release. Cells without treatment were used as a negative control. To understand the effect of autophagy inhibition in hBN cytotoxicity, some A549-ALI cultures were pre-incubated (at least 1 h) with wortmannin (100 nM, ThermoFisherScientific, Switzerland), a pharmacological inhibitor of cellular autophagy. The cultures were then exposed to hBN (10 µg cm^{-2}) for 24 h and LDH release was measured. For LDH assay, 50 µL of recovered supernatant from the basolateral side was distributed in a 96-well plate and LDH assay was performed using CytoTox96 non-radioactive cytotoxicity kit (Promega, Germany). The absorbance of each well was measured at 490 nm with a microplate reader (Mithras2 Plate reader, Berthold Technologies, Germany). Absorbance values were corrected with blank (cell medium only) and normalized to untreated controls. The experiments were carried out with a minimum of three biological and three technical replicates. Results were shown as a percentage of viable cells compared to the highest LDH release in positive control.

Cytotoxicity and Oxidative Stress Assays–Evaluation of Epithelial Barrier Integrity: The barrier integrity of A549-ALI cultures was determined by measuring the transepithelial electrical resistance (TEER) of the cultures before exposure and 24 h after exposure to hBN. At least three measurements in different regions of the transwell cultures were recorded from each sample. The TEER (Ω × cm^2) values were calculated by subtracting the resistance of a cell-free transwell insert and multiplying it by the surface area (1.13 cm^2) of the insert.[76] The experiments were carried out at least three times and the mean value was presented.

Cytotoxicity and Oxidative Stress Assays–Total Cellular Reactive Oxygen Species (ROS) Content: H2DCF/DCF ROS assay was performed to measure the total ROS level in the cells. Briefly, A549-ALI cultures were exposed to hBN for 24 h. Following exposure, the cells were harvested by trypsinization for 25 min and pelleted by centrifugation (200 *xg*, 5 min). The cell pellet was stained with µM H2-DCF (Invitrogen, Switzerland) and incubated for 30 min in the dark at 37°C. After incubation, DCF fluorescence in the cells was recorded using an Attune flow cytometer operated with Attune software (ThermoFisherScientific, U.S.A.). Data were analyzed using FCS Express software.

Cytotoxicity and Oxidative Stress Assays–Lipid Oxidation: Lipid peroxidation was determined after exposure of A549-ALI cultures to hBN at the indicated concentrations for 24 h. After exposure, the cells were harvested by trypsinization for 25 min followed by centrifugation (200 *xg*, 5 min). The cells were resuspended in PBS containing 2 µM C11-$BODIPY^{581/591}$ (ThermoFisherScientific, Switzerland) and incubated for 30 min in the dark at 37°C. The C11-$BODIPY^{581/591}$ analysis was performed using the Attune flow cytometer operating Attune software (ThermoFisherScientific, U.S.A.).

Lipid Accumulation: Lipid accumulation in A549-ALI cultures was determined by staining the cells with $BODIPY^{493/503}$ (Thermo Fisher Scientific) for 30 min at 37°C, imaging by CLSM (LSM780, Zeiss, Germany), and quantification of the increase in $BODIPY^{493/503}$ intensity in hBN-treated cultures with respect to untreated controls. Briefly, the A549-ALI cultures were exposed to hBN at indicated concentrations for 24 h. Following exposure, the samples were collected and processed for flow cytometry and confocal imaging as described above. The confocal images were processed using Zen software (Black or Blue Edition version 2.6).

For lysosomal colocalization after $BODIPY^{493/503}$ staining, the cells were probed with 100 nM of LysoTracker deep red (ThermoFisherScientific, Switzerland) for 30 min followed by counterstaining with DAPI for 10 min. The slides for confocal imaging were prepared in the same way as described above.

Autophagy Assay: The autophagy induction in A549-ALI cultures was determined by using an autophagy detection kit (Cat. no. 139 484, Abcam,

Germany). To this end, A459-ALI cultures were exposed to hBN (5 and 10 µg cm^{-2}) or rapamycin (500 nM; positive control) and maintained for 24 h. Following exposure, the cells were washed with PBS and processed for sample preparation for flow cytometry and confocal imaging. For flow cytometry, the cells were first harvested by trypsinization and then stained with a dual detection reagent and incubated for 30 min as suggested by the manufacturer. Following incubation, the cellular fluorescence for the green detection reagent was analyzed using an Attune flow cytometer operated with Attune software (ThermoFisherScientific, U.S.A.). For confocal microscopy, the cells were directly stained in the transwell membranes with the dual detection reagent for 30 min, followed by fixing the cells with 4% formaldehyde. Finally, the cells in the transwell membrane were mounted on glass slides as described above and imaged under a CLSM (LSM780, Zeiss, Germany). The images were processed using Zen software (Black or Blue Edition version 2.6).

Immunofluorescence: A549 cells were cultured on transwell membranes under air-liquid interface conditions and then exposed to hBN nanosheets (10 µg cm^{-2}) or chloroquine (100 µM, positive control) (InvitroFit, InvivoGen, Germany) for 24 h. Cells exposed to the culture medium only were used as a negative control. Following exposure, cells were washed thrice using 1 × PBS, fixed with Histofix (4% formaldehyde, Sigma-Aldrich, Germany) for 15 min, and permeabilized with 0.2% Triton X-100 for 15 min at room temperature (RT). Next, cells were blocked using 10% goat serum (Sigma-Aldrich, Germany) supplemented with 0.2% Triton X-100 at RT for 1 h. Then, the cells were incubated overnight at 4 °C with primary antibodies: rabbit anti-LC3B (1:1000, ab192890, Abcam, Germany) and mouse anti-LAMP1 (1:100, ab25630, Abcam, Germany). The following day, cells were washed thrice with 1 × PBS and then incubated with Alexa Fluor 488-conjugated goat anti-rabbit (1:400, Invitrogen, Switzerland) and Alexa Fluor 633-conjugated goat anti-mouse (1:400, Invitrogen, Switzerland) secondary antibodies (1:1000) for 1 h at RT. The cells were further incubated with nuclear stain, DAPI (1:1000, Invitrogen) for 10 min at RT. Finally, the samples were washed and mounted on glass slides using Mowiol488 (Sigma-Aldrich, Germany) and left overnight at 37 °C. The immunofluorescence staining was visualized with a CLSM (LSM 780, Zeiss, Germany) at 63x magnification. The images were processed using Zen software (version 2.6).

Interleukin 8 (IL-8) ELISA: A549-ALI cultures were exposed to hBN nanosheets (10 µg/cm^2) for 24 h. Following exposure, the basolateral medium was collected and stored at −80°C. IL-8 content was determined using an uncoated IL-8 ELISA kit (Invitrogen, Switzerland) by following manufacturer instructions. Absorbance was measured at 450 nm using a microplate reader (Mithras^2 Plate reader, Berthold Technologies, Germany). Results were expressed as pg/mL of released IL-8, based on at least three independent experiments.

Statistical Details: The results shown were derived from at least three independent experiments. Data were presented as mean values ± standard deviation (SD). GraphPad Prism 5 (GraphPad) and Origin 2022 were used for the statistical analysis. One-way ANOVA followed by Dunnett's or Tukey's post hoc analysis was applied as indicated. A statistical significance was defined as $*p < 0.05$, $**p < 0.01$, $***p < 0.001$, and $****p < 0.0001$ compared to the negative controls.

Supporting Information

Supporting Information is available from the Wiley Online Library or from the author.

Acknowledgements

Funding for this research was received from the European Union (EU) 8th Framework Program for Research and Technological Development, Graphene Flagship project (H2020-FET- GrapheneCore3 – #881603) and MACRAME (Grant agreement number – 101092686 and State Secretariat for Education, Research and Innovation (SERI) no 23.00141). A part of the work was supported by an internal grant from the Cantonal Hospital St. Gallen and the Swiss Federal Laboratories for Materials Science and Technology (Empa/KSSG 15/12). The authors would like to acknowledge BeDimensional Spa (Italy), an associated partner in the Graphene Flagship project, for providing hBN nanosheets used in the present study. The authors would like to thank Professor Ester Vázquez Fernández-Pacheco (University of Castilla-la Mancha (UCLM) for helpful discussions on the physicochemical properties of hBN nanosheets. Some images were created with BioRender.com.

Open access funding provided by ETH-Bereich Forschungsanstalten.

Conflict of Interest

The authors declare no conflict of interest.

Author Contributions

G.G. designed the study, performed the cell-based experiments, analyzed data, and wrote the paper; Z.W. contributed to the cellular assays; V.M.K. performed protocol development and sample preparation for TEM and SEM, TEM imaging, and TEM and SEM data analysis and compilation of cells and particles; A.G. supported in ICP-MS analysis and performed SEM/EDX imaging; P. W. reviewed & edited the manuscript, and acquired funding. T.B. acquired funding, conceptualized and coordinated the study, analyzed data, and contributed in writing the paper. All co-authors edited and approved the final version of the paper.

Data Availability Statement

The data that support the findings of this study are available from the corresponding author upon reasonable request.

Keywords

2D materials, air-liquid interface exposure, lipid droplets, lipid homeostasis, lipophagy

Received: September 16, 2023
Revised: November 29, 2023
Published online:

[1] B. Fadeel, C. Bussy, S. Merino, E. Vázquez, E. Flahaut, F. Mouchet, L. Evariste, L. Gauthier, A. J. Koivisto, U. Vogel, C. Martín, L. G. Delogu, T. Buerki-Thurnherr, P. Wick, D. Beloin-Saint-Pierre, R. Hischier, M. Pelin, F. Candotto Carniel, M. Tretiach, F. Cesca, *ACS Nano* **2018**, *12*, 10582.
[2] S. Chortarea, O. C. Kuru, W. Netkueakul, M. Pelin, S. Keshavan, Z. Song, B. Ma, J. Gómes, E. V. Abalos, L. A. Visani de Luna, T. Loret, A. Fordham, M. Drummond, N. Kontis, G. Anagnostopoulos, G. Paterakis, P. Cataldi, A. Tubaro, C. Galiotis, I. Kinloch, B. Fadeel, C. Bussy, K. Kostarelos, T. Buerki-Thurnherr, M. Prato, A. Bianco, P. Wick, *J. Hazard. Mater.* **2022**, *435*, 129053.
[3] A. F. Rodrigues, L. Newman, D. Jasim, S. P. Mukherjee, J. Wang, I. A. Vacchi, C. Ménard-Moyon, A. Bianco, B. Fadeel, K. Kostarelos, C. Bussy, *Adv. Sci.* **2020**, *7*, 1903200.
[4] H. F. Krug, P. Wick, *Angew. Chem., Int. Ed.* **2011**, *50*, 1260.
[5] J. Li, H. Zeng, Z. Zeng, Y. Zeng, T. Xie, *ACS Biomater. Sci. Eng.* **2021**, *7*, 5363.
[6] C. R. Dean, A. F. Young, I. Meric, C. Lee, L. Wang, S. Sorgenfrei, K. Watanabe, T. Taniguchi, P. Kim, K. L. Shepard, J. Hone, *Nat. Nanotechnol.* **2010**, *5*, 722.

[7] J. Lee, A. V. Ravichandran, J. Mohan, L. Cheng, A. T. Lucero, H. Zhu, Z. Che, M. Catalano, M. J. Kim, R. M. Wallace, A. Venugopal, W. Choi, L. Colombo, J. Kim, *ACS Appl. Mater. Interfaces* **2020**, *12*, 36688.
[8] J. Deb, U. Sarkar, *Appl. Surf. Sci.* **2021**, *541*, 148657.
[9] J. Gu, Y. Guo, X. Yang, C. Liang, W. Geng, L. Tang, N. Li, Q. Zhang, *Composites, Part A* **2017**, *95*, 267.
[10] S. Sumitani, Y. Nagasaki, *Polymer Journal* **2012**, *44*, 522.
[11] I. V. Feiner, K. R. Pulagam, K. B. Uribe, R. Passannante, C. Simó, K. Zamacola, V. Gómez-Vallejo, N. Herrero-Álvarez, U. Cossío, Z. Baz, M. M. Caffarel, C. H. Lawrie, D. J. Vugts, L. Rejc, J. Llop, *J. Mater. Chem. B* **2021**, *9*, 410.
[12] A. Zaboronok, P. Khaptakhanova, S. Uspenskii, R. Bekarevich, L. Mechetina, O. Volkova, B. J. Mathis, V. Kanygin, E. Ishikawa, A. Kasatova, D. Kasatov, I. Shchudl, T. Sycheva, *S. Taskaev and A. Matsumura Pharmaceutics* **2022**, *14*, 761.
[13] B. Singh, G. Kaur, P. Singh, K. Singh, B. Kumar, A. Vij, M. Kumar, R. Bala, R. Meena, A. Singh, A. Thakur, A. Kumar, *Sci. Rep.* **2016**, *6*, 35535.
[14] L. Li, J. Li, Y. Shi, P. Du, Z. Zhang, T. Liu, R. Zhang, Z. Liu, *ACS Nano* **2019**, *13*, 13843.
[15] Y. Zhang, H. G. Kang, H. Z. Xu, H. Luo, M. Suzuki, Q. Lan, X. Chen, N. Komatsu, L. Zhao, *Adv. Mater.* **2023**
[16] L. Li, K. Dai, J. Li, Y. Shi, Z. Zhang, T. Liu, J. Xie, R. Zhang, Z. Liu, *Biomaterials* **2021**, *268*, 120587.
[17] T. Lu, L. Wang, Y. Jiang, C. Huang, *J. Mater. Chem. B* **2016**, *4*, 6103.
[18] M. Pelin, S. Sosa, M. Prato, A. Tubaro, *Nanoscale* **2018**, *10*, 15894.
[19] I. Basinas, A. S. Jiménez, K. S. Galea, M. V. Tongeren, F. Hurley, *Annals of Work Exposures and Health* **2018**, *62*, 639.
[20] A. Erdely, M. Dahm, B. T. Chen, P. C. Zeidler-Erdely, J. E. Fernback, M. E. Birch, D. E. Evans, M. L. Kashon, J. A. Deddens, T. Hulderman, S. A. Bilgesu, L. Battelli, D. Schwegler-Berry, H. D. Leonard, W. McKinney, D. G. Frazer, J. M. Antonini, D. W. Porter, V. Castranova, M. K. Schubauer-Berigan, *Part. Fibre Toxicol.* **2013**, *10*, 53.
[21] L. Ou, B. Song, H. Liang, J. Liu, X. Feng, B. Deng, T. Sun, L. Shao, *Part. Fibre Toxicol.* **2016**, *13*, 57.
[22] S. P. Mukherjee, G. Gupta, K. Klöditz, J. Wang, A. F. Rodrigues, K. Kostarelos, B. Fadeel, *Small* **2020**, *16*, 1907686.
[23] L. Ahlinder, J. Henych, S. W. Lindström, B. Ekstrand-Hammarström, V. Stengl, L. Österlund, *RSC Adv.* **2015**, *5*, 59447.
[24] V. Kodali, J. R. Roberts, E. Glassford, R. Gill, S. Friend, K. L. Dunn, A. Erdely, *J. Mater. Res.* **2022**, *37*, 4620.
[25] A. B. Kakarla, I. Kong, *Nanomaterials* **2022**, *12*, 2069.
[26] L. Horvath, A. Magrez, D. Golberg, C. Zhi, Y. Bando, R. Smajda, E. Horvath, L. Forro, B. Schwaller, *ACS Nano* **2011**, *5*, 3800.
[27] V. K. Kodali, J. R. Roberts, M. Shoeb, M. G. Wolfarth, L. Bishop, T. Eye, M. Barger, K. A. Roach, S. Friend, D. Schwegler-Berry, B. T. Chen, A. Stefaniak, K. C. Jordan, R. R. Whitney, D. W. Porter, A. D. Erdely, *Nanotoxicology* **2017**, *11*, 1040.
[28] X. Xin, M. Barger, K. A. Roach, L. Bowers, A. B. Stefaniak, V. Kodali, E. Glassford, K. L. Dunn, K. H. Dunn, M. Wolfarth, S. Friend, S. S. Leonard, M. Kashon, D. W. Porter, A. Erdely, J. R. Roberts, *NanoImpact* **2020**, *19*, 100235.
[29] H. Barosova, A. G. Maione, D. Septiadi, M. Sharma, L. Haeni, S. Balog, O. O'Connell, G. R. Jackson, D. Brown, A. J. Clippinger, P. Hayden, *ACS Nano* **2020**, *14*, 3941.
[30] C. A. Poland, R. Duffin, I. Kinloch, A. Maynard, W. A. Wallace, A. Seaton, V. Stone, S. Brown, W. MacNee, K. Donaldson, *Nat. Nanotechnol.* **2008**, *3*, 423.
[31] C. Ge, Y. Li, J. J. Yin, Y. Liu, L. Wang, Y. Zhao, C. Chen, *NPG Asia Mater.* **2012**, *4*, e32.
[32] E. Aldieri, I. Fenoglio, F. Cesano, E. Gazzano, G. Gulino, D. Scarano, A. Attanasio, G. Mazzucco, D. Ghigo, B. Fubini, *Journal of Toxicology and Environmental Health, part A* **2013**, *76*, 1056.
[33] V. Kodali, K. S. Kim, J. R. Roberts, L. Bowers, M. G. Wolfarth, J. Hubczak, X. Xin, T. Eye, S. Friend, A. B. Stefaniak, S. S. Leonard, M. Jakubinek, A. Erdely, *Small* **2022**, *18*, 2203259.
[34] M. A. Lucherelli, X. Qian, P. Weston, M. Eredia, W. Zhu, P. Samorì, H. Gao, A. Bianco, A. von dem Bussche, *Adv. Mater.* **2021**, *33*, 2103137.
[35] H. Lin, S. Peng, S. Guo, B. Ma, M. A. Lucherelli, C. Royer, S. Ippolito, P. Samorì, A. Bianco, *Small* **2022**, *18*, 2107652.
[36] I. Kooter, M. Ilves, M. Gröllers-Mulderij, E. Duistermaat, P. C. Tromp, F. Kuper, P. Kinaret, K. Savolainen, D. Greco, P. Karisola, J. Ndika, H. Alenius, *ACS Nano* **2019**, *13*, 6932.
[37] T. L. Moore, L. Rodriguez-Lorenzo, V. Hirsch, S. Balog, D. Urban, C. Jud, B. Rothen-Rutishauser, M. Lattuada, A. Petri-Fink, *Chem. Soc. Rev.* **2015**, *44*, 6287.
[38] C. B. Anders, J. J. Chess, D. G. Wingett, A. Punnoose, *Nanoscale Res. Lett.* **2015**, *10*, 448.
[39] N. Basu, M. S. Satya Bharathi, M. Sharma, K. Yadav, A. S. Parmar, V. R. Soma, J. Lahiri, *Nanomaterials* **2021**, *11*, 622.
[40] W. Wang, Z. Li, A. J. Marsden, M. A. Bissett, R. J. Young, *2D Mater.* **2021**, *8*, 035058.
[41] K. T. Al-Jamal, K. Kostarelos, *Carbon Nanotubes: Methods and Protocols* **2010**, 123.
[42] M. Kucki, L. Diener, N. Bohmer, C. Hirsch, H. F. Krug, V. Palermo, P. Wick, *J. Nanobiotechnol.* **2017**, *15*, 46.
[43] S. Keshavan, G. Gupta, S. Martin, B. Fadeel, *Nanotoxicology* **2021**, *15*, 1125.
[44] G. Gupta, F. Cappellini, L. Farcal, R. Gornati, G. Bernardini, B. Fadeel, *Part. Fibre Toxicol.* **2022**, *19*, 33.
[45] P. Cronholm, H. L. Karlsson, J. Hedberg, T. A. Lowe, L. Winnberg, K. Elihn, I. O. Wallinder, L. Möller, *Small* **2013**, *9*, 970.
[46] G. J. Rosenthal, D. R. Germolec, M. E. Blazka, E. Corsini, P. Simeonova, P. Pollock, L.-Y. Kong, J. Kwon, M. I. Luster, *J. Immunol.* **1994**, *153*, 3237.
[47] B. S. Qazi, K. Tang, A. Qazi, *International journal of inflammation* **2011**, *2011*, 908468.
[48] B. Domi, K. Bhorkar, C. Rumbo, L. Sygellou, S. N. Yannopoulos, R. Barros, R. Quesada, J. A. Tamayo-Ramos, *Int. J. Mol. Sci.* **2021**, *22*, 567.
[49] Z. Li, Y. Zhang, C. Chan, C. Zhi, X. Cheng, J. Fan, *ACS Nano* **2018**, *12*, 2764.
[50] M. C. Morissette, P. Shen, D. Thayaparan, M. R. Stämpfli, *European Respiratory Journal* **2015**, *46*, 1451.
[51] C. W. Agudelo, G. Samaha, I. Garcia-Arcos, *Lipids in Health and Disease* **2020**, *19*, 122.
[52] P. Mahavadi, I. Henneke, C. Ruppert, L. Knudsen, S. Venkatesan, G. Liebisch, R. C. Chambers, M. Ochs, G. Schmitz, C. Vancheri, W. Seeger, *Toxicol. Sci.* **2014**, *142*, 285.
[53] G. Schmitz, G. Müller, *J. Lipid Res.* **1991**, *32*, 1539.
[54] B. Qiu, M. C. Simon, *Bio-protocol* **2016**, *17*, e1912.
[55] J. A. Olzmann, P. Carvalho, *Nat. Rev. Mol. Cell Biol.* **2019**, *20*, 137.
[56] T. Amen, D. Kaganovich, *Cell Rep.* **2021**, *35*, 109237.
[57] E. Jarc, T. Petan, *The Yale Journal of Biology and Medicine* **2019**, *92*, 435.
[58] Z. Doumandji, R. Safar, M. Lovera-Leroux, S. Nahle, H. Cassidy, D. Matallanas, B. Rihn, L. Ferrari, O. Joubert, *Cell Biol. Toxicol.* **2020**, *36*, 65.
[59] Z. Chen, S. Han, P. Zheng, D. Zhou, S. Zhou, G. Jia, *Nanoscale* **2020**, *12*, 5973.
[60] R. Ma, X. Cai, Y. Zhou, X. Liu, D. Wu, H. Zheng, Y. Pan, J. Jiang, S. Xu, Q. Xie, J. Jiang, *Environ. Sci.: Nano* **2022**, *9*, 105.
[61] A. M. Thelen, R. Zoncu, *Trends Cell Biol.* **2017**, *27*, 833.

[62] A. S. Zembroski, C. Andolino, K. K. Buhman, D. Teegarden, *Frontiers in Oncology* **2021**, *11*, 576326.
[63] X. Li, J. Wu, X. Sun, Q. Wu, Y. Li, K. Li, Q. Zhang, Y. Li, E. D. Abel, H. Chen, *Stem Cell Rep.* **2020**, *14*, 420.
[64] J. Y. Guo, E. White, *Autophagy* **2013**, *9*, 1636.
[65] M. A. Pabon, K. C. Ma, A. M. Choi, *Am. J. Respir. Cell Mol. Biol.* **2016**, *54*, 636.
[66] R. Singh, S. Kaushik, Y. Wang, Y. Xiang, I. Novak, M. Komatsu, K. Tanaka, A. M. Cuervo, M. J. Czaja, *Nature* **2009**, *458*, 1131.
[67] Y. Fu, N. Chen, Z. Wang, S. Luo, Y. Ding, B. Lu, *Cell Res.* **2021**, *31*, 965.
[68] O. Meçe, D. Houbaert, M. L. Sassano, T. Durré, H. Maes, M. Schaaf, S. More, M. Ganne, M. García-Caballero, M. Borri, J. Verhoeven, M. Agrawal, K. Jacobs, G. Bergers, S. Blacher, B. Ghesquière, M. Dewerchin, J. V. Swinnen, S. Vinckier, M. S. Soengas, P. Carmeliet, A. Noël, P. Agostinis, *Nat. Commun.* **2022**, *13*, 2760.
[69] X. Zhao, S. Wei, Z. Li, C. Lin, Z. Zhu, D. Sun, R. Bai, J. Qian, X. Gao, G. Chen, Z. Xu, *Cell Death Dis.* **2019**, *10*, 127.
[70] M. Mauthe, I. Orhon, C. Rocchi, X. Zhou, M. Luhr, K. J. Hijlkema, R. P. Coppes, N. Engedal, M. Mari, F. Reggiori, *Autophagy* **2018**, *14*, 1435.
[71] E. F. Blommaart, U. Krause, J. P. Schellens, H. Vreeling-Sindelárová, A. J. Meijer, *Eur. J. Biochem.* **1997**, *243*, 240.
[72] X. Wei, C. Hogstrand, G. Chen, W. Lv, Y. Song, Y. Xu, Z. Luo, *Environ. Sci. Technol.* **2021**, *55*, 4943.
[73] S. Zhang, X. Peng, S. Yang, X. Li, M. H. M., S. Wei, J. Liu, G. He, H. Zheng, L. Yang, H. Li, *Cell Death Dis.* **2022**, *13*, 132.
[74] Z. Q. Lan, Z. Y. Ge, S. K. Lv, B. Zhao, C. X. Li, *Cell Death Discovery* **2023**, *9*, 229.
[75] J. D. Pressly, M. Z. Gurumani, J. T. Varona Santos, A. Fornoni, S. Merscher, H. Al-Ali, *Am. J. Physiol.: Cell Physiol.* **2022**, *322*, C468.
[76] D. Korejwo, S. Chortarea, C. Louka, M. Buljan, B. Rothen-Rutishauser, P. Wick, T. Buerki-Thurnherr, *NanoImpact* **2023**, *29*, 100452.